1. INTRODUCTION

1.1 Inlet Total Pressure Distortion

Inlet flow distortions in fluid machinery are defined as variations of flow properties as a function of space and time and have been of major concern to turbomachinery designers for decades. These deviations from a steady uniform distribution of the flow properties can include variations in swirl, vorticity, turbulence, total and static pressures, velocity, temperature, flow angle, and fluid density (1, 2).

Inlet total pressure distortions are the most common type of distortion in axial-flow compressors. They can be created in aircraft gas turbine applications by a number different sources, such as extreme aircraft maneuvers, engine-inlet configuration, inlet boundary interactions, wakes from nearby aircraft, and atmospheric turbulence, as shown in Figure 1.1.

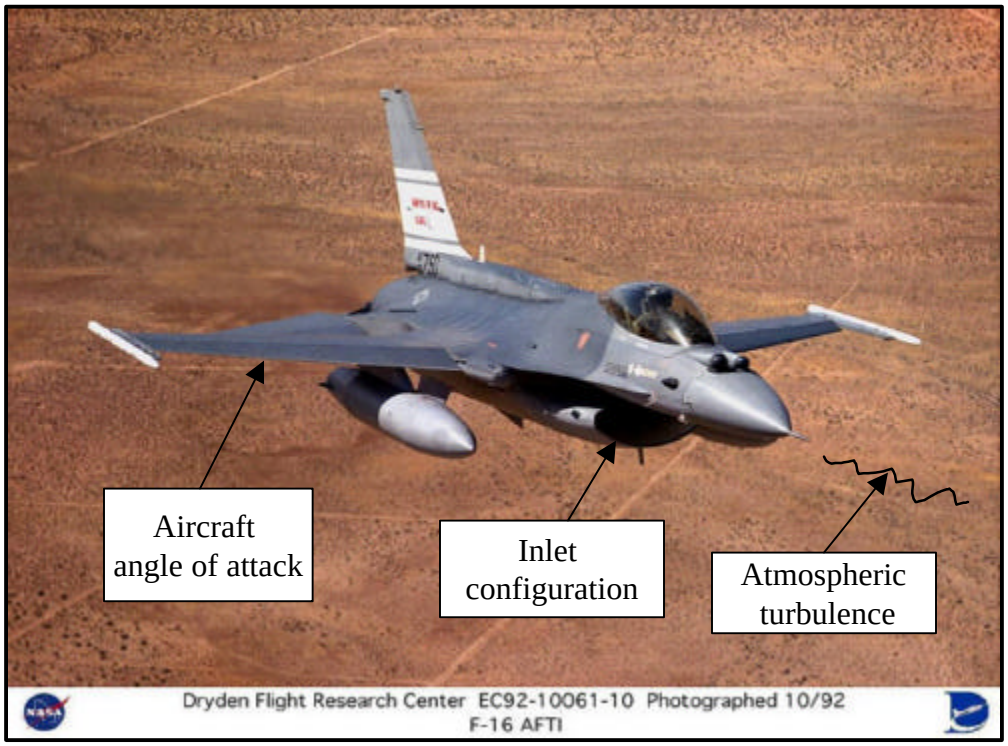

Figure 1.1: Factors Contributing to Inlet Total Pressure Distortion in Aircraft Engines.

Compressors in stationary applications are subject to inlet total pressure distortion as well; for example, in industrial installations with poorly designed upstream bends or in highly circuitous Naval inlet systems (3).

The consequences of a compressor operating in a pressure distorted inflow include performance degradation, unsteady blade forces, vibration, and, very importantly, a reduction in stall margin when compared to a compressor with no distortion. This phenomenon is shown in Figure 1.2 for a high-speed compressor (4).

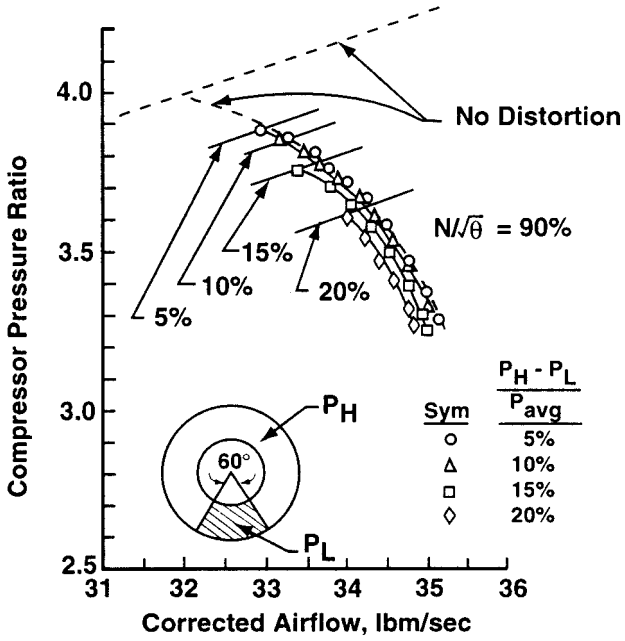

Figure 1.2: Sample Performance Map for an Axial-Flow Compressor (Kimzey, 1977).

Compressor stall margin is typically defined as the difference between the compressor pressure ratios at stall (straight dotted line in Figure 1.2) and at the operating point divided by the compressor pressure ratio of the normal operating point (points in Figure 1.2) along a constant corrected airflow line (5). Note in Figure 1.2 how increasing the strength, or total pressure loss, of the distortion will progressively reduce the stall margin of the compressor for a given operating point. Figure 1.2 also depicts how the

entire speed line shifts to lower values of mass flow rate and total pressure rise to compensate for lower corrected airflow. As the strength of the distortion (magnitude of flow total pressure loss across it) increases the speed lines will shift performance to a progressively lower corrected rotor speed.

Compressors may also experience surge when subject to a severe distortion. Surge is a large-scale event involving flow reversal through the entire compressor. Surge only occurs after a stall condition is attained in one or more compressor blade rows. Results of surge include power loss, engine flame out, and internal component damage due to high temperature air passing upstream through the cold section of the engine.

The present study concentrated on the measurement of the steady inlet flow angles of a low-speed isolated rotor and its unsteady rotor wake response relative to the circumferential position of distortion screens of constant extent and varying intensity. The experimental arrangement, testing procedures, and results of this investigation are described in the following sections.

1.2 Fundamental Cascade Aerodynamics

The objective of this section is to define terminology, definitions, notation, and sign convention used in two-dimensional linear cascade analysis as described by Yocum (6). Figure 1.3 illustrates the absolute and relative flow velocities in an axial-flow cascade.

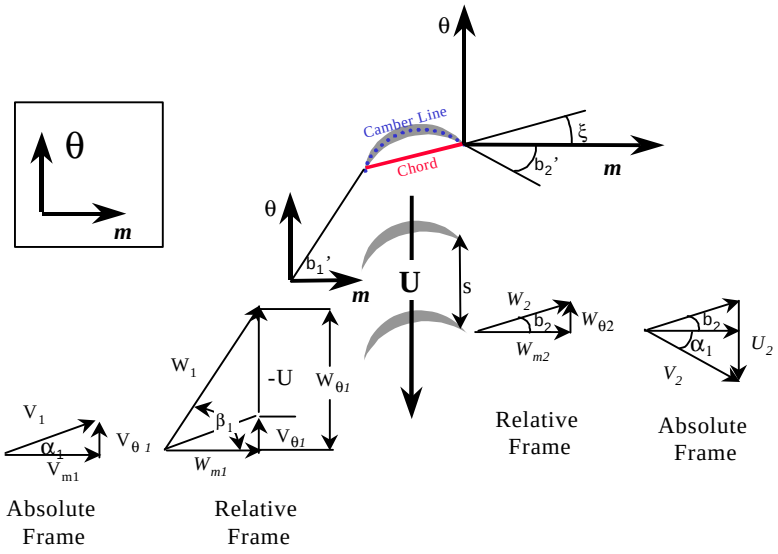

Figure 1.3 Axial-flow Compressor Cascade Geometry and Velocity Triangles.

As the cascade blades are moving with velocity U in the -q direction, it is convenient to view the fluid velocity from the perspective of a cascade blade in order to simplify blade row performance evaluation. This is known as switching from the absolute frame to the relative frame of reference. The absolute velocities and flow angles are expressed as V_i and α_i, respectively, and the relative velocities and flow angles are expressed as W_i and β_i, respectively. In order to relate absolute to relative reference frames or vice versa, one need only apply the vector sum as shown in Equation **(1.1)**.

$$\overline{\mathbf{W}} = \overline{\mathbf{V}} - \overline{\mathbf{U}} \qquad \textbf{(1.1)}$$

The camber line is that line which represents the mid-point of the blade between its pressure and suction sides at every point along the airfoil. The length of the camber line is often referred to as the camber length. The blade angles (β'_1) and (β'_2), also called the metal angles, are those between the meridional axis (m) and the line tangent to the camber

line at the blade leading and trailing edges, respectively. The angle formed between the chord line and the meridional axis is referred to as the stagger angle (ξ).

$$i = \beta_1 - \beta'_1 \quad \textbf{(1.2)}$$

$$\alpha = \beta_1 - \xi \quad \textbf{(1.3)}$$

$$\theta' = \beta'_1 - \beta'_2 \quad \textbf{(1.4)}$$

These geometry definitions include the incidence angle (i), angle of attack (α), and camber angle (θ'). The camber angle (θ') is the ideal amount of turning a cascade would impose on a flow if the flow entered tangent to the camber line.

All data for this research were obtained in the stationary frame of reference with respect to laboratory coordinates, using a combination of steady-state and high-response unsteady probes.

2. LITERATURE REVIEW

Several hundred documents exist in the literature which describe testing and research performed in an effort to improve compressor response to inlet total pressure distortion. Due to this extreme number of relevant publications, this literature review will emphasize steady-state circumferential pressure distortion in axial-flow fans and compressors.

2.1 Pressure Distortion Simulation Techniques

The two dominant forms of pressure distortion are classified as circumferential and radial with respect to the machine axis, as shown in Figure 1.4.

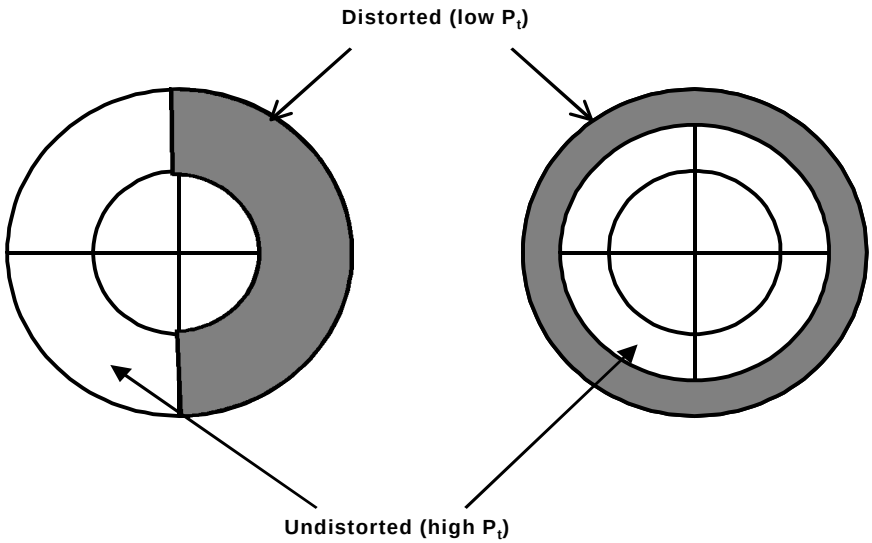

Figures 1.4: Circumferential and Radial Total Pressure Distortion Patterns.

Circumferential distortions are viewed as being more critical than radial distortions due to the production of a disturbance normal to the airfoil motion, and resulting effects on angle of attack and stall margin.

Screens are typically used to impose steady-state total pressure distortions on fans and compressors based on the simplicity of application and cost-effectiveness. The effect of fluid viscosity on the flow is to produce a viscous static pressure drop across the screen grid, as well as a deflection of streamlines to the screen outer edges (7).

It is important to note that a distortion screen installed in front of a rotor will not produce an identical circumferential pressure defect pattern downstream at the aerodynamic interface plane of the rotor inlet due to upstream fluid communication between the screen and rotor. Although ideally the screens would produce "square-wave" pressure patterns at the inlet of the rotor, in reality there are transition regions at the edges of the screen. Therefore, total pressure at the rotor inlet as viewed in the relative frame will never be a "step function" but rather a continuous variation as the blade passes downstream of the screen.

Two basic parameters characterize a steady circumferential inlet total pressure distortion, these being 1) the circumferential extent, and 2) the distortion intensity or magnitude of total pressure loss through the distorted flow region.

2.2 Distortion and Wake Testing in Axial Flow Fans and Compressors

Many studies have been conducted in both the stationary and relative frames of measurement to investigate how fluid flow through a fan or compressor varies due to circumferential inlet total pressure distortions. The literature review resulted in five general publication categories with application to distortion and wake response. The first group of papers concerns inlet flow condition and blade lift response to distortion. The second group of papers concerns blade response to a transient blade incidence angle above the steady-state stalling angle. The third category concerns wake analysis with respect to variations in incidence angle or operating point on the map. The fourth category discusses the phenomena of the suction side total pressure profile appearing as a jet, or pressure excess, in the stationary frame of reference. The fifth category is limited to one paper discussing the effect of inlet total pressure distortion on inlet flow conditions and three-dimensional wake response.

As previously stated, a number of fan and compressor studies have been performed with regard to variations in inlet flow conditions due to distortion. Soeder and Bobula (8) investigated the effect of steady circumferential total pressure distortion on flow characteristics entering an aircraft engine using classical screens. They found that for a transonic turbofan engine, maximum and minimum flow yaw angles in the absolute frame occurred within the constant intensity distortion sector of the flowfield as opposed to at the screen edges. They also found the yaw angle is usually the largest in the hub region for the screen configurations they tested. This yaw angle variation increased in magnitude as the flow approached the engine inlet. Increasing the screen blockage increased the yaw angle variation. They also discovered that the inlet pitch angle variation in the plane of the distortion is much smaller than the yaw angle variation, as would be expected for purely circumferential distortions.

Cousins (9) analyzed the unsteady blade surface pressures due to circumferential inlet total pressure distortion in a low-speed axial-flow compressor rig using on-rotor pressure transducers and a telemetry system. Stationary high-response probes were employed to capture wake pressure variations during rotating stall. He showed that it was feasible to develop a transfer function describing the dynamic blade response using data from on-rotor pressure measurements and Fourier transform techniques.

Gauden (10) investigated the performance and stalling behavior of a low-speed axial-flow compressor subjected to three different circumferential inlet distortion levels. He used steady-state instrumentation in the stationary frame of reference and high-response pressure transducers mounted on the blades. He discovered that distortion screens reduced the mass flow rate through the compressor due to their low porosity and precipitated stall at a more open throttle valve setting than for undistorted operation.

Gauden found that with respect to the direction of rotor motion, a sharp increase in axial velocity was observed as the distorted segment was approached, implying a decreased angle of attack at the blade leading edge. This was due to flow blockage created by the distortion screens. As the blades passed circumferentially through the

distorted flow region behind the screens, the axial velocity was reduced until the angle of attack was maximized, and then returned to its undistorted value at the trailing edge of the screen. The shape of the circumferential velocity profile remained roughly the same as the flow rate was decreased using a throttle valve.

Dancy (11) tested the performance and stalling behavior of a low-speed axial-flow compressor with circumferential inlet flow distortion. Similar to the results of Gauden for the same test rig, he discovered that axial velocity increased nearly 10 % as the leading edge of the screen was approached, then fell off sharply and leveled out. An opposite effect occurred at the "departure" end of the screen with respect to rotor rotation. He found that velocities in the undistorted segments of a partially-distorted inlet were higher than the constant flow velocity for a clean inlet. Although the compressor was set to produce the same volumetric flow rate in both cases, the flow rate increase in the undistorted region was insufficient to return the compressor to its original, undistorted volumetric flow rate. As a result, the undistorted compressor always had a higher flow rate. As the back pressure was increased, the flow rates for the distorted and undistorted compressors approached the same value due to a decreased axial velocity and, subsequently, a decreased total pressure drop across the screen. He also found rotating stall for RAF-6 airfoils to originate at the hub of the blade.

The second literature category, blade response to an unsteady incidence that exceeds the steady-state stalling angle, is presented next. Sexton (12) investigated the dynamic stalling characteristics of low-speed axial-flow compressor blades using blade-mounted transducers and a multi-channel radio telemetry system. High incidence angles and stalling were induced using a distortion screen mounted in front of the IGV. This screen had a mesh of sufficiently low porosity as to insure incidence angles greater than the steady-state stalling angle. This allowed separation of the blade boundary layer behind the distorted region and reattachment in the undistorted region during each revolution. Sexton then developed a transfer function between the quasi-steady total pressure loss forcing function and the dynamic pressure loss response function. This transfer function in

turn described the dynamic response of the rotor blade row flow and made possible the prediction of response to a given inlet distortion for a rotating stall model.

Neal (13) used a multi-channel FM telemetry system in conjunction with miniature blade-mounted transducers to investigate low-speed rotor blade lift response due to circumferential inlet flow distortions. He found that normalized lift for an undistorted compressor decreases as the volumetric flow rate is decreased and angle of attack is correspondingly increased. He explained this unusual behavior by noting that although the coefficient of lift increases with an increase in angle of attack, the decrease in volumetric flow rate causes a decrease in absolute lift. The normalized lift of the distorted compressor first increased and then decreased as flow rate was decreased. He explained this as being due to competing effects of changes in angle of attack, changes in volumetric flow rate, and changes in the level of distortion as the back pressure was increased by closing a downstream discharge valve. He presented an analysis of rotor blade lift and rotor inlet dynamic pressure for a rotor cycle during which the blade experienced a far greater incidence than the steady-state stalling angle.

Neal found that although the blade did eventually stall as it passed well into a distortion, the delay in the inception of stall was significant, with partial stalling of the instrumented rotor blade just prior to the blade's exit from the distorted segment. This corresponded closely to the highest angle of attack on the rotor blade during the rotor cycle. The dynamic stall event was typically characterized by a lift overshoot, which then collapsed and returned to the undistorted lift value after the trailing edge of the screen. This indicated boundary layer reattachment. The phenomenon of a blade experiencing an incidence angle beyond the steady-state stalling angle without stalling was also observed by Melick (14) and Henderson and Horlock (15), and was postulated to be a function of the rotor blade lift response.

The third literature category will focus on wake analysis with respect to variations in incidence or operating point on the map. The wake of a rotor blade may be defined as the downstream region of pressure and momentum defect due to boundary layer

separation in an adverse pressure gradient (16). In addition, in viscous flows over a body a wake exists even if the flow is not separated or has a favorable pressure gradient. The wake defect may be defined as the difference between the local velocity in the wake and the freestream velocity between the blade passages. The near wake is the region where the defect is of the same order of magnitude as the freestream velocity and the far wake is defined as where the defect is an order of magnitude less than the freestream mean velocity (17).

Lakshminarayana, et al. (18) studied the effects of rotation and blade incidence on the properties of a low-speed fan rotor wake. They defined a wake semi-width at half the depth on both the pressure and suction sides of the wake and non-dimensionalized them by the rotor blade spacing in the circumferential direction. They found that the wake defect was reduced as rotor rotational speed increased and that the axial velocity wake defect was highest at the hub. Higher rotor speed gave lower axial velocity defect, and higher loading increased the axial velocity defect (or decreased the downstream decay rate of the axial velocity defect). The wake semi-width at a fixed loading did not change with an increase in rotor rotational speed. In addition, they found that wake semi-width was lower at lower loading and the growth was less rapid.

Shreeve and Neuhoff (19) found the wake of a small, transonic single-stage axial compressor to broaden at reduced throttle settings and increased blade speed. Henderson and Shen (20) investigated the influence of unsteady rotor response on a distorted flow field in a low speed axial flow rotor. They found that as the rotor was loaded by decreasing the flow coefficient, the boundary layer thickness, wake defect magnitude, and wake width all increased.

Reynolds, et al. (21) found the wake of an isolated low-speed rotor to be three-dimensional in nature with an appreciable radial velocity due to an imbalance in the radial pressure gradient and centrifugal forces. They defined wake semi-widths on the rotor pressure and suction surfaces to obtain a width parameter which was non-dimensionalized by blade spacing.

Ravindranath and Lakshminarayana (22) performed an experimental study of the three-dimensional characteristics of the mean relative frame velocity in the wake of a moderately loaded compressor rotor blade. They defined a non-dimensional semi-width parameter as the sum of the characteristic widths on the pressure and suction surfaces normalized by the semi-blade spacing. They found the effect of blade loading was to sustain the wake asymmetry to a much larger extent downstream of the blade trailing edge. Increased loading also increased the velocity defect magnitude, slowed the decay rate, and induced higher radial velocities. They found the wake width to vary considerably in the radial direction. The width increased towards the hub- and annulus-walls, which was attributed to the complex interaction of the wake, hub-, or annulus-wall boundary layers, and secondary flows (tip vortex in the case of the annulus-wall). They found the static pressure to vary across the wake as well as in the wake near the blade trailing edge due to inviscid effects, which is not reflected in total pressure plots. The static pressure was highest at the center of the wake. They compared the variation of the first two Fourier coefficients of velocity with downstream distance and studied the averaged Fourier coefficients and scatter of the harmonic content in the rotor wake.

Reynolds and Lakshminarayana (17) studied the three-dimensional relative flow characteristics of a lightly loaded low-speed rotor wake. They found that increased loading slowed the decay rates of the axial and tangential mean velocity components and radial velocities in the wake. They found that wake width increased with loading, and that only in the far wake was it acceptable to assume a negligible static pressure variation. Also, the axial and tangential components of mean velocity were highly asymmetric about the wake centerline, a trait which was more pronounced for increased loading. They found the wake width to increase with radial position about mid-radius and speculated that this may have resulted from large radial transport of mass, momentum, and energy.

Muhlemann (23) performed experiments that showed strong radial variation of the wake with the largest mean velocity defects and wake widths near the hub and tip regions.

He also found a more rapid decay of wake width as blade loading was increased, a result verified by Ufer (24).

Kerrebrock, et al. (25) found considerable randomness in absolute exit flow angle at several radii in the wake of a blowdown transonic rotor, even when wake pressure and velocity profiles were quite sharp. They suggested the source of time dependence as random effects from the hub and tip regions influencing the entire blade span.

The fourth category included discussions of the phenomena of the suction side total pressure profile appearing as a jet, or pressure excess, in the wake. Shreeve, et al. (26, 27) found impact pressures to be a jet on the suction side of the blades in the wake of a transonic rotor. Shreeve and Neuhoff (19) found the absolute velocity in the wake of a transonic rotor to have a larger magnitude on the suction side of the blades, a phenomena which was more evident at the hub where blade and flow velocities were subsonic. Schmidt and Okiishi (28) found a higher axial velocity downstream of the suction side of the blade when measured in the stationary frame, a phenomena which was, again, more pronounced at the hub region. Lakshminarayana, et al. (18) found the axial velocity to be higher on the suction side of the wake of a low-speed fan rotor blade when measured in the stationary frame of reference. Ravindrath and Lakshminarayana (22) found higher total relative velocity and stagnation pressure profiles downstream of the suction side of a low-speed rotor blade, indicating that the phenomena of a suction side jet is not limited to stationary measurements. Ng and Epstein (29) also discovered the presence of a suction side jet during total pressure measurements in the wake of an axial-flow transonic fan.

Cherrett and Bryce (30) studied the unsteady three-dimensional exit flow fields in the stationary frame of a single-stage transonic fan, comparing random stagnation pressure unsteadiness to ensemble-averaged stagnation pressure unsteadiness. They found that in the stationary frame it is possible for stagnation pressures to be higher on the suction, rather than the pressure, surface side of the passage, and for a wake in the relative frame to appear as a jet (pressure excess) in the stationary frame. In the wake region, the stagnation pressure rose rapidly from a pressure trough on the pressure surface side of the

rotor wake, to a pressure peak on the suction surface side of the wake. The magnitude of the suction side peak relative to the mean level was two to three times that of the pressure trough. The point in the wake region where the stagnation pressure rose above time-averaged values corresponded approximately to the position of maximum random unsteadiness. A second stagnation pressure trough occurred on the suction surface side of the wake followed by a peak comparable to the strength of that attained within the suction surface side of the rotor wake. Wake unsteadiness was found to be three to four times that elsewhere in the blade passage, with peak unsteadiness at mid-pitch. Ensemble-averaged wake stagnation pressures indicated little change in amplitude with increased compressor loading at the same speed, with the exception of the lower blade spans toward the hub where rotor inlet Mach numbers approached unity.

The fifth category is limited to one paper discussing the effect of inlet total pressure distortion on blade inlet flow conditions and three-dimensional wake response. Colpin and Kool (31) studied the propagation of a non-uniform upstream flow field through a low-speed axial-flow compressor stage rotor. Circumferential total pressure distortion was created using a grid which was rotatable with respect to the stationary instrumentation. They found that the distortion was indicated more strongly in flow angles than velocities downstream of the rotor. They found that as a blade passed into a distortion the boundary layer on the suction side thickened due to the increase in loading. Moving further into the distorted region, the axial velocity outside of the wake increased due to increasing blockage caused by the wake. A strong reduction in the relative outlet flow angle corresponded to stronger centrifugation, or radial flow, in the blade wakes. Moving further still into the distorted region, the blade wake reached its maximum thickness indicating boundary layer separation on the suction side while the freestream axial velocity mean value increased to compensate for the additional boundary layer blockage. When reaching the distortion trailing edge, the boundary layer on the blades tended to reattach, inducing a thinner wake. After the blade passed through the distorted region, the investigators noted a reduction in wake circumferential extent and depth, as

well as a slight increase in axial velocity. Colpin and Kool also noted that the flow turbulence increased at the inlet and exit of the rotor while in the distorted region. As the suction side boundary layer separated, the turbulence level suddenly grew due to the development of a large wake.

It is interesting to note that Colpin and Kool also experienced incidence angles greater than the quasi-steady stall value. A strong decrease in wake dynamic pressure corresponding to the maximum incidence angle reinforced the observation of blade dynamic stall. The increase in inlet relative flow angle did not induce an immediate growth of the boundary layers, implying that a time lag is introduced into the boundary layer response as shown in references (32, 33, 34).

The limitations of the Colpin and Kool experiment with respect to the present investigation were that data was only taken at mid-span for one screen and one operating point. The rotor blade row also had adjacent IGV and stator rows, and the probes were located too far from the rotor, allowing a significant circumferential flow redistribution between the probes and the blade row.

Conclusions from Literature Review

There is a lack of fundamental wake data, where an isolated rotor experiences a dynamic distortion condition in the relative frame of reference, particularly when the steady-stalling incidence angle is exceeded. A more comprehensive study of the dynamic wake response for a variety of distortion intensities, operating points, blade shapes, and measurement spans is necessary. There is no literature associated with pre-stall blade exit total pressure surveys with respect to a distorted region.

The following chapters of this document will present the procedures and results of this investigation in the following manner. Chapter III describes the experimental arrangement, instrumentation, calibration, and data acquisition and analysis procedures. Chapter IV presents the results of the experiments and an appropriate discussion, Chapter V presents the conclusions, and Chapter VI provides recommendations for future experiments.